Organization of the MADS Box from Human SRF Revealed by Tyrosine Perturbation

ARTICLE *in* THE JOURNAL OF PHYSICAL CHEMISTRY B · JANUARY 2015

Impact Factor: 3.3 · DOI: 10.1021/jp508897p · Source: PubMed

THE JOURNAL OF PHYSICAL CHEMISTRY B

Article

pubs.acs.org/JPCB

Organization of the MADS Box from Human SRF Revealed by Tyrosine Perturbation

Barbora Profantová,[†,‡] Yves-Marie Coïc,[§] Václav Profant,[‡] Josef Štěpánek,*[,‡] Vladimír Kopecký, Jr.,[‡] Pierre-Yves Turpin,[†] Bernard Alpert,[∥] and Christian Zentz[∥]

[†]Lab. Jean Perrin, CNRS UMR 8237, UPMC Université Paris 6, 4 place Jussieu, 75252 Paris Cedex 05, France

[‡]Institute of Physics, Faculty of Mathematics and Physics, Charles University in Prague, Ke Karlovu 5, 121 16 Prague 2, Czech Republic

[§]Unité de Chimie des Biomolécules, Institut Pasteur, UMR CNRS 3523, 75724 Paris, France

[∥]ER12, UPMC Université Paris 06, 4 place Jussieu, 75252 Paris Cedex 05, France

Supporting Information

ABSTRACT: MADS box family transcription factors are involved in signal transduction and development control through DNA specific sequence recognition. The DNA binding domain of these proteins contains a conservative 55−60 amino acid sequence which defines the membership of this large family. Here we present a thorough study of the MADS segment of serum response factor (MADS^{SRF}). Fluorescence, UV-absorption, and Raman spectroscopy studies were performed in order to disclose its behavior and basic functional properties in an aqueous environment. The secondary structure of MADS^{SRF} estimated by analysis of Raman spectra and supported by CD has revealed only the C-terminal part as homologous with those of free core-SRF, while the N-terminal part has lost the stable α-helical structure found in both the free core-SRF and its specific complex with DNA. The three tyrosine residues of the MADS^{SRF} were used as spectroscopic inner probes. The effect of environmental conditions, especially pH variations and addition of variously charged quenchers, on their spectra was examined. Two-component fluorescence quenching was revealed using factor analysis and corresponding Stern−Volmer constants determined. Factor analysis of absorbance and fluorescence pH titration led to determination of three dissociation constants pK_a1 = 6.4 ± 0.2, pK_a2 = 7.3 ± 0.2, and pK_a3 = 9.6 ± 0.6. Critical comparison of all experiments identified the deprotonation of His193 hydrogen bonded to Tyr195 as a candidate for pK_a1 (and that of Tyr158 as a candidate for pK_a2). Within MADS^{SRF}, His193 is a key intermediary between the N-terminal primary DNA binding element and the hydrophobic C-terminal protein dimerization element.

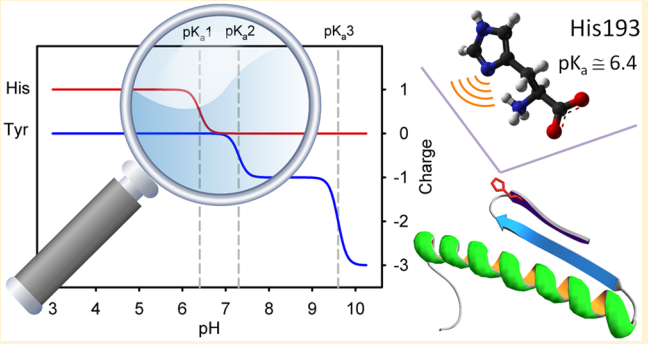

INTRODUCTION

MADS box transcription factors show an extensive homology of a 55−60 amino acid sequence called the MADS box.[1,2] The MADS acronym is derived from four of the originally identified members: Minichromosome maintenance 1, Agamous, Deficiens, and Serum response factor (SRF).[3] Members of the MADS box family are involved in signal transduction and development control in yeasts, fungi, plants, and animals.

The MADS-box segment forms a part of a core domain of many members of the family. Its N-terminal basic part forms the primary DNA binding element, whereas the C-terminal hydrophobic segment forms part of a protein dimerization domain. Available structural data of core domains of several MADS-box proteins in complexes with target DNA have revealed a high homology of the structure but with topology differences in DNA binding.[4−9]

In the case of core-SRF of about a hundred amino acid residues, the MADS-box (SRF 142−197) takes part in the activities of DNA specific recognition,[10] protein dimerization, and recruitment of accessory factors.[11−13] In complex with core-SRF, the targeted oligonucleotide is continuously switching between bend and linear conformers.[14] A dynamic pairing between both partners with specific electric oscillations is characteristic of this complex.[15] The SRF MADS-box (MADS^{SRF}) motif (residues 142−197) may underline basic functional properties common to its protein family. The high structure conservation of these complexes, the invariance of Lys163, Arg164, Gly167, Lys170, Lys171, and Glu174, and the conservation of a hexameric hydrophobic patch spanning

Received: September 3, 2014
Revised: December 12, 2014
Published: January 5, 2015

DOI: 10.1021/jp508897p
J. Phys. Chem. B 2015, 119, 1793−1801

residues 183 to 188 suggest that analogous structural scaffolds may be used to elicit similar but distinctive interaction mechanisms with DNA targets.[3] The X-ray structure of core-SRF dimer bound to DNA[4] revealed that its C-terminal part consists of two β sheets (residues βI, 182−188; residues βII, 194−198) connected by a β loop and one α-helix (residues αII, 209−219), whereas its N-terminal part is composed of a N-extension (residues 132−152) and an α-helix (residues αI, 153−179)—see Figure 1.

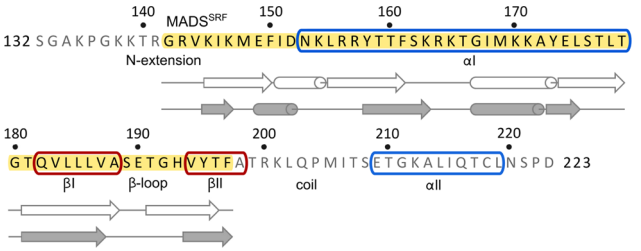

Figure 1. Core-SRF with marked MADS^{SRF} sequence. The secondary structure elements were marked according to the crystal structure.[4] Chou and Fasman[27] (white) and GOR[28] (gray) estimations of the secondary structures are depicted down the sequence.

Here we present a study of the synthesized MADS^{SRF} segment in order to disclose its behavior and basic functional properties in aqueous environment. A thorough study in using fluorescence, UV-absorption, and Raman spectroscopy was performed. The three tyrosine residues of the MADS^{SRF} [3] were used as spectroscopic inner probes.[16] To distinguish their individual contributions to the spectra and their further characterization, the effect of small changes of the environmental conditions, especially the effect of pH variations and concentration of charged quenchers, was examined.

EXPERIMENTAL PROCEDURES

Peptide Synthesis and Purification. The 56 amino acid sequence reproducing human MADS^{SRF} was used for synthesis (see Figure 1).[3]

The synthesis was carried out according to the Fmoc/tBu solid-phase strategy[17] on a 433A peptide synthesizer (Applied Biosystems), using a Fmoc polystyrene AM RAM resin (RAPP Polymere). Other chemicals were obtained from Applied Biosystems, except for piperidine used for Fmoc deprotection which was purchased from Sigma. 2-(1*H*-9-Azabenzotriazole-1-yl)-1,1,3,3-tetramethyluronium hexafluorophosphate (HATU)/diisopropylethylamine (DIPEA) were used as coupling reagents, and Fmoc amino acid derivatives were single coupled with an 8-fold molar excess with regard to the resin. N-Terminal acetylation was achieved on the peptide resin at the end of the synthesis with acetic anhydride. Cleavage from the solid support and deprotection of the amino acid side chains were accomplished in one step by treatment with 92.5% trifluoroacetic acid, 2.5% ethanedithiol, 2.5% triisopropylsilane, and 2.5% water (v/v/v/v) for 3 h at room temperature. After filtration of the resin, the cleavage mixture was poured into ice-cold diethyl ether. The peptide was then recovered by filtration of the precipitate and lyophilized. The deprotected crude peptide was dissolved with a mixture of aqueous trifluoroacetic acid/acetonitrile (25%) and directly purified by reverse-phase medium pressure liquid chromatography (MPLC) on a preparative column packed with 100 Å, 20 μm, C18 Nucleoprep packing (Macherey-Nagel), by applying a linear gradient (0.6%/min) of acetonitrile in 0.08% aqueous trifluoroacetic acid over 60 min at a 20 mL/min flow rate. MADS^{SRF} was eluted from a column at 42% acetonitrile under these conditions.

A major coproduct showing a mass of 1431.80 Da was observed by reverse-phase high pressure liquid chromatography (RP-HPLC) analysis in the crude peptide and remains important after MPLC. Amino acid composition of this side-product was assessed by amino acid analysis upon isolated material and matched to that of the truncated fragment Leu186−Phe197. We hypothesized a difficult coupling step of Leu185 due to a stretch of hydrophobic amino acids and a Glu190 transamidation side reaction with piperidine, which could explain the delta mass of +67 with regard to the theoretical molecular weight of the acetylated fragment. An additional step of purification by RP-HPLC on a nucleosil 5 μm, C18, 300 Å semipreparative column was necessary, using the same eluents with a 0.5%/min linear gradient over 20 min at a 6 mL/min flow rate.

The purified peptide was quantified by amino acid analysis (isolated peptide yield 0.72%) and characterized by positive ion electrospray ionization mass spectrometry. The experimental data (6511.83 ± 0.29 Da) was consistent with the expected mass (6511.71 Da).

Raman Spectroscopy. MADS^{SRF} samples (9 mg/mL) in 25 mM cacodylate buffer pH 7.0 and acetate buffer pH 4.5, placed in a temperature stabilized microcell of 12 μL internal volume, were excited by the 488.0 nm/500 mW Ar^+ laser (Coherent). Raman spectra were recorded on a T64000 CCD Raman spectrometer (Jobin-Yvon) in standard 90° geometry. Data were recorded in the spectral range from 800 to 1750 cm^{-1} and accumulated 200 × 3 s. The effective spectral resolution was ~4 cm^{-1}. A neon glow-lamp spectrum was recorded after every analyzed sample and the Raman shift values were refined by using an automatic recalibration procedure. Spectral contributions from solvent, light scattered by walls of a glass microcell and background represented by a sixth degree polynomial, were subtracted using a least-squares fit.

Fluorescence Spectroscopy. Fluorescence measurements were performed on an SLM Aminco-Bowman series 2 luminescence spectrometer. The excitation wavelengths were 278 and 275 nm for quenching and pH titration experiments, respectively. The excitation and emission spectral bandwidths were 4 nm.

Fluorescence emission spectra at a concentration of 1×10^{-5} M preserved an unchanged profile over a 1 month period at room temperature.

Recorded fluorescence spectra were corrected for the Rayleigh and Raman scattering as well as for the small changes of the sample concentration resulting from the addition of quenchers or pH changing solutions. The inner filter effect was corrected taking the optical density at the excitation (OD_{EX}) and emission (OD_{EM}) wavelengths into consideration in accordance with ref 18:

$$f = 10^{(OD_{EX}+OD_{EM})/2} \quad (1)$$

The maximum optical density was 0.2 in the spectral range of investigated fluorescence emission.

For the pH dependency of MADS^{SRF}, the spectra were measured in the pH range from 3.0 to 9.5 at a temperature of 20 °C and a concentration of 5×10^{-6} M. Measurement of

DOI: 10.1021/jp508897p
J. Phys. Chem. B 2015, 119, 1793−1801

higher pH values was not possible due to the precipitation of the sample. The pH was altered by addition of small amounts of HCl (Merck) or KOH (Normapur) solutions to the sample and measured on a pH meter IQ170G (IQ Scientific Instruments) equipped with a stainless steel pH probe.

Fluorescence quenching was investigated for 1×10^{-5} M MADS^{SRF} in 25 mM cacodylate buffer pH 6.5 by adding increasing amounts of ionic quenchers I^- or Cs^+. A small amount of $S_2O_3^{2-}$ ($\sim 10^{-4}$ M) was added to the iodide anion solution to prevent I^{3-} formation.

Fluorescence excitation spectra for 1×10^{-5} M MADS^{SRF} were measured in deionized water at pH 5.7 for emissions 293, 304, and 325 nm.

UV−vis Absorbance Spectroscopy. Spectra of 5×10^{-6} M MADS^{SRF} at various pH's were recorded immediately after acquisition of the fluorescence spectra (see the "Fluorescence Spectroscopy" section) on a Bio-Tek Kontron UVIKON 923 spectrophotometer. The optical path length was 1 cm. Acquired spectra were corrected for a baseline shift and for dilution caused by addition of pH changing solutions.

Theory—Factor Analysis. Generally, a factor analysis (FA) enables distinguishing among individual spectral components in the property dependent spectral series, i.e., decrease of the fluorescence caused by addition of quencher or spectral change by alteration of pH in our case. The sets of experimental spectra were subjected to FA using the singular value decomposition (SVD) algorithm. A set of N spectra is decomposed into a set of orthogonal normalized spectral profiles

$$Y_i(\lambda) = \sum_{j=1}^{M} V_{ij} W_j S_j(\lambda) \tag{2}$$

where the normalized coefficients V_{ij} quote relative portions of the jth spectral profile S_j in the original spectra Y_i. The singular numbers W_j stand for the statistical weights of spectral profiles. The spectral profiles are ordered to reach a descending succession of singular values until the terms on the right side of eq 2 are sufficient to approximate the original spectral set within an experimental error. The number of necessary terms M, the factor dimension, represents the number of independent spectral profiles resolved in the analyzed spectral set. (A detailed explanation of FA can be found in ref 19.)

Theory—Fluorescence Quenching. In the case of MADS^{SRF}, two spectral components $F_I(\lambda)$ and $F_{II}(\lambda)$ were resolved in quenching experiments. According to the Stern−Volmer relation,[18,20] the overall fluorescence spectrum $Y_i(\lambda)$ in the presence of quencher is given by the relation

$$Y_i(\lambda) = F_I(\lambda)/(1 + K_I^Q \cdot C_i^Q) + F_{II}(\lambda)/(1 + K_{II}^Q \cdot C_i^Q) \tag{3}$$

where C_i^Q is the concentration of the quencher Q and K_I^Q and K_{II}^Q are the corresponding Stern−Volmer constants. Simultaneously, $F_I(\lambda)$ and $F_{II}(\lambda)$ can be well approximated as linear combinations of two SVD spectral profiles

$$F_I(\lambda) = \Sigma^2_{j=1} r_j^I \cdot S_j(\lambda), \quad F_{II}(\lambda) = \Sigma^2_{j=1} r_j^{II} \cdot S_j(\lambda) \tag{4}$$

where r_j^I and r_j^{II} are the coefficients of linear combination. Considering eq 2 for $Y_i(\lambda)$ and the orthogonality of SVD spectral profiles $S_j(\lambda)$, a final set of $2 \times N$ equations was obtained:

$$W_j V_{ij} = r_j^I/(1 + K_I^Q \cdot C_i^Q) + r_j^{II}/(1 + K_{II}^Q \cdot C_i^Q), \quad i = 1, 2, ..., N, \quad j = 1, 2 \tag{5}$$

The six unknown parameters (K_I^Q, K_{II}^Q, r_j^I, r_j^{II}; $j = 1, 2$) can be solved by a simultaneous nonlinear least-squares fit of the right sides of these equations to the left ones.

Theory—pH Titration. To obtain pK_a values of the MADS^{SRF}, the approach published in ref 21 was altered for the presence of three pK_a values in correspondence with four spectral components resolved in the pH titration (instead of only one pK_a, used in the article). Therefore,

$$Y_i(\lambda) = C_i^A \cdot F^A(\lambda) + C_i^B \cdot F^B(\lambda) + C_i^C \cdot F^C(\lambda) + C_i^C \cdot F^D(\lambda) \tag{6}$$

where $F^A(\lambda)$, $F^B(\lambda)$, $F^C(\lambda)$, and $F^D(\lambda)$ are the spectral components forming the original spectrum $Y_i(\lambda)$ proportionally to their current relative occurrences C_i^A, C_i^B, C_i^C, and C_i^D given by

$$\begin{aligned} C_i^A &= 1/(1 + 10^{pH-pK_a1} + 10^{2pH-pK_a1-pK_a2} + 10^{3pH-pK_a1-pK_a2-pK_a3}) \\ C_i^B &= C_i^A \cdot 10^{pH-pK_a1} \\ C_i^C &= C_i^B \cdot 10^{pH-pK_a2} \\ C_i^D &= C_i^C \cdot 10^{pH-pK_a3} \end{aligned} \tag{7}$$

The four spectral components can be approximated as linear combinations of SVD spectral profiles

$$\begin{aligned} F^A(\lambda) &= \sum_{j=1}^{M} r_j^A S_j(\lambda) \\ F^B(\lambda) &= \sum_{j=1}^{M} r_j^B S_j(\lambda) \\ F^C(\lambda) &= \sum_{j=1}^{M} r_j^C S_j(\lambda) \\ F^D(\lambda) &= \sum_{j=1}^{M} r_j^D S_j(\lambda) \end{aligned} \tag{8}$$

where r_j represent the coefficients of linear combination. Due to the orthogonality of spectral profiles, a final set of $M \times N$ equations is obtained as

$$W_j V_{ij} = r_j^A \cdot C_i^A + r_j^B \cdot C_i^B + r_j^C \cdot C_i^C + r_j^D \cdot C_i^D, \quad i = 1, 2, ..., N, \quad j = 1, 2, ..., M \tag{9}$$

The results of the pH titration experiment consisted of two spectral sets, fluorescence and UV absorption; SVD of each spectral set provided three spectral components applicable in further analysis. This analysis was a least-squares fit of the right sides in eq 9 to the left ones using eq 7, simultaneously for fluorescence and absorption data. The fit thus included $2 \times 3 \times N$ equations and 27 unknown parameters, i.e., pK_a1, pK_a2, and pK_a3 constants, 12 coefficients r_j^A, r_j^B, r_j^C, and r_j^D, $j = 1, 2, 3$, for fluorescence spectra, and 12 coefficients for spectra of absorption.

DOI: 10.1021/jp508897p
J. Phys. Chem. B 2015, 119, 1793−1801

RESULTS

Raman Spectra of MADS^{SRF}. Figure 2 displays the Raman spectrum of MADS^{SRF} at pH 7.0 and 20 °C. Several prominent

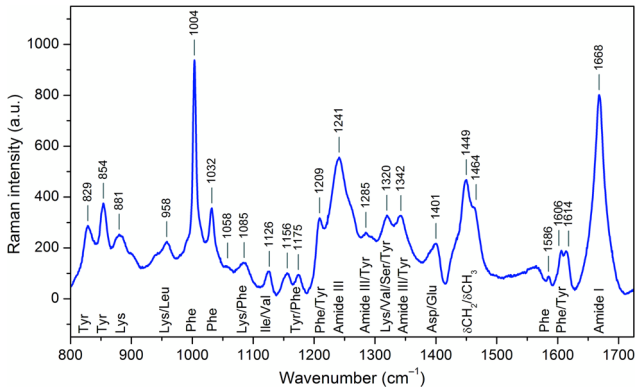

Figure 2. Raman spectrum of MADS^{SRF} at pH 7.0 at a temperature of 20 °C. Band assignment was done in accordance with the literature.[22−24]

bands corresponding to vibrations of amino acids with aromatic side chains can be observed (e.g., 1004, 1032, and 1586 cm^{-1} of Phe and 829, 854, and 1614 cm^{-1} of Tyr[22−24]). The intensity of the tyrosine doublet I_{854}/I_{828} = 1.3 reflects that the majority of tyrosines are exposed to the solvent and participate in weak or moderate H-bonding (both as donors and acceptors).[25] Nevertheless, the spectrum is dominated by vibrations of the peptide backbone, represented by amide I (in the region 1630−1700 cm^{-1}) and amide III (the region 1220−1340 cm^{-1}) bands, together with bending vibrations of CH_2 groups (at 1449 and 1464 cm^{-1}). The classical pattern of the β-sheet conformation is demonstrated by the maximum of the amide I band at 1668 cm^{-1} and the amide III band at 1241 cm^{-1}.[22−24] Especially the amide I band is very narrow pointing on the rigidity of the peptide fold. Estimation of the secondary structure content was achieved by using the least-squares analysis method in the region of the amide I and amide III bands.[26] We have found 64−69% of β-sheet content, 22−25% of β-turn content, and ∼2% of α-helix content. The structural difference between MADS^{SRF} at pH 4.5 and 7.0 was negligible. Very good agreement between estimation of the secondary structure content from the amide I and amide III regions was reached (see Table 1).

The determined secondary structure content, particularly the small amount of α-helix, was independently confirmed by measurements and analysis of electronic circular dichroism (CD) spectra (see Figure S5 and Table S1 in the Supporting Information).

As the Raman spectrum does not change with pH, there is a weak effect of temperature by heating the MADS^{SRF} solution from 5 to 50 °C connected with ∼4% β-sheet increase (data not shown).

Tyr Fluorescence of MADS^{SRF}. In the absence of Trp in the sequence of MADS^{SRF}, the three Tyr residues serve as inner spectroscopic probes. The fluorescence emission spectrum (Figure 3) displays a three-humped emission composed of a

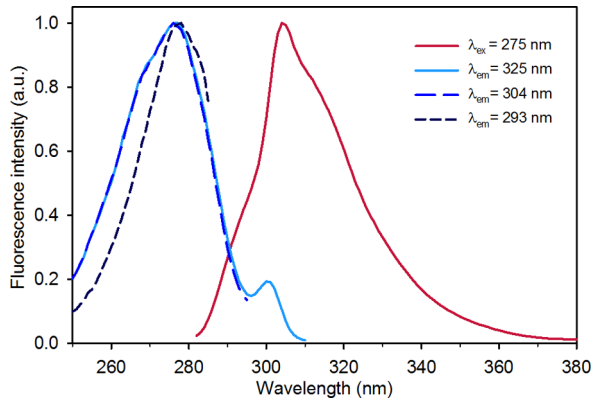

Figure 3. Normalized fluorescence emission (red) and excitation (blue) spectra of the MADS^{SRF} in water. The emission spectrum was excited at 275 nm. The excitation spectra were recorded for emissions at 293, 304, and 325 nm.

shoulder on the shorter wavelengths (ca. 293 nm) of the spectrum, a peak at 303 nm, and a weak shoulder on the longer wavelengths of the spectrum (ca. 320 nm).

The quantum yield of MADS^{SRF} fluorescence was only slightly varying (±8%) at the concentration within the 9.9 × 10^{-6} and 1.1 × 10^{-6} M interval at pH 3.4. The fluorescence profile of emission remained unchanged.

Fluorescence excitation spectra of the MADS^{SRF} were recorded for fluorescence emitted at 293, 304, and 325 nm (Figure 3). While the excitation spectrum for emission at 293 nm has a simple shape with a maximum at 277 nm, the spectra for emissions at 304 and 325 nm manifest an additional shoulder at ∼268 nm and the latter also a weak band at ∼300 nm. These additional features indicate the presence of tyrosine either in its deprotonated form (tyrosinate) or engaged in a strong or unusual hydrogen bond.[29−31]

Fluorescence Quenching by Iodide and Cesium. In order to determine the accessibility to solvent and charges of the Tyr residues of MADS^{SRF}, quenching by Cs^+ and I^- was performed at pH 6.5. To find out the dimensionality of the quenching effect on fluorescence spectra, the sets of MADS^{SRF} fluorescence spectra obtained for various concentrations of

Table 1. Estimation of the Secondary Structure Content of MADS^{SRF} at Different pH's by the Pattern Recognition Least-Squares Method[a] for Amide I (LSA-I) and Amide III (LSA-III) Bands[26] [b]

	pH 4.5		pH 6.95	
	LSA-I	LSA-III	LSA-I	LSA-III
α-helix	2 (1) ± 5%	2 (1) ± 5%	2 (1) ± 5%	2 (1) ± 5%
β-sheet	67 (38) ± 4%	65 (36) ± 6%	69 (39) ± 4%	64 (36) ± 6%
β-turn	23 (13) ± 2%	21 (12) ± 5%	23 (13) ± 2%	22 (12) ± 5%
other	10 (6) ± 2%	9 (5) ± 4%	11 (6) ± 2%	9 (5) ± 4%

[a]Given standard deviations are calculated as standard deviations of the used reference set. [b]Numbers in parentheses correspond to amino acids included in each structure.

DOI: 10.1021/jp508897p
J. Phys. Chem. B 2015, 119, 1793−1801

either of the quenchers were subjected to SVD (for details, see the Experimental Procedures). Only two singular values above the noise level indicated that the factor dimension is 2 (data not shown). This means that all fluorescence spectra in the presence of I^- and Cs^+ can be reconstructed as linear combinations of just two spectral profiles, S_1 and S_2 (Figure 4).

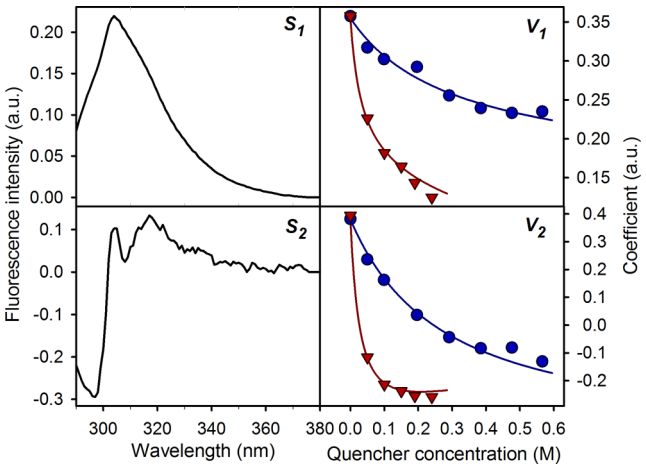

Figure 4. Factor analysis of the emission spectra of $MADS^{SRF}$ fluorescence quenched by I^- (red triangles) and Cs^+ (blue circles). For each concentration of quencher, the fluorescence spectrum of $MADS^{SRF}$ is a sum of two spectral profiles S_j (left), both multiplied by corresponding coefficients V_{ij} (right).

By a fit of V_{i1} and V_{i2} dependences to the Stern–Volmer equation[20] (for details, see the "Theory—Fluorescence Quenching" section), we obtained the same two major components of the emission spectrum for both quenchers, F_I and F_{II}, each of them characterized with a certain Stern–Volmer constant (K^Q), a measure of the quenching efficacy. In particular, $K_I^I = 33.2 \pm 7.0\ M^{-1}$ and $K_I^{Cs} = 3.4 \pm 0.5\ M^{-1}$ were obtained for the spectral component F_I and $K_{II}^I = 2.5 \pm 0.8\ M^{-1}$ and $K_{II}^{Cs} = 0.2 \pm 0.2\ M^{-1}$ for the component F_{II}. Figure 5

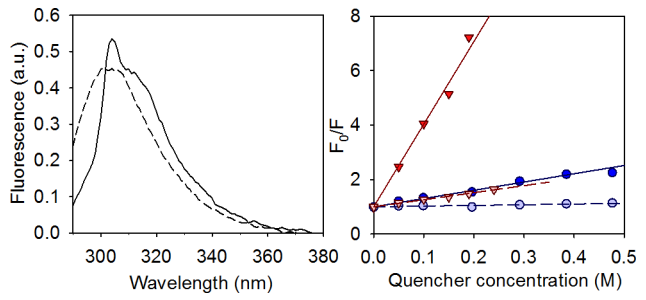

Figure 5. Two differently quenched spectral components distinguished by SVD (left) and their Stern–Volmer representation (right). Solid lines correspond to the more efficiently quenched F_I component and dashed lines to the second component F_{II}. Circles and red lines correspond to Cs^+, and triangles and blue lines, to I^- quenching.

shows the spectral components and their practically linear quenching characteristics in the Stern–Volmer representation. The more efficiently quenched component F_I possesses a more complicated shape (with a maximum at 304 nm) and is more distinctive with respect to the emission spectrum of $MADS^{SRF}$ (Figure 3). The spectral shape of the less efficiently quenched component F_{II} is simpler. The ratios of Stern–Volmer constants of iodide over cesium K^I/K^{Cs} are nearly the same for both components F_I and F_{II} and amount to slightly more than 10. This is in good correspondence with the other fluorescence quenching studies, where Cs^+ was found to quench the fluorescence of aromatic molecules approximately 10 times less efficiently than I^-.[32,33] The Stern–Volmer constant ratio K_I/K_{II} remains similar independent of the quencher charge.

As I^- and Cs^+ provide a pair of quenchers with opposite charges and similar diffusion parameters,[34] it could be anticipated that due to their different charge they would quench preferentially tyrosines surrounded by an environment of opposite charge. Contrary to this assumption, the same ratio of the Stern–Volmer constant K^I/K^{Cs} was observed for both components F_I and F_{II}. This indicates that the quenching mainly resolves the global solvent accessibility and does not differentiate between various microenvironments of the Tyr residues.

Absorbance and Fluorescence pH Titration. To better understand the role of variations of $MADS^{SRF}$ charges on the environment of its Tyr residues, pH titration was performed. In general, increasing the pH from 3 to 7 causes a decrease of the fluorescence intensity; further increase of the pH causes the fluorescence intensity to drop even more significantly, and at pH 9.5, the $MADS^{SRF}$ precipitates (the peptide denaturation is irreversible, data not shown).

To obtain more specific information about the changes induced by pH variations in the range below the precipitation limit, sets of fluorescence and absorption spectra measured at pH ranging from 3.0 to 9.4 were subjected to SVD separately. The factor dimension was found to be 3 in both cases. By a joint fit of coefficients obtained from SVD of fluorescence and absorption spectra, respectively (see Figure S1 in the Supporting Information; for details, see the "Theory—pH Titration" section), four different spectral components and three corresponding kinds of acido-basic equilibria were determined. The obtained dissociation constant values are $pK_a1 = 6.4 \pm 0.2$, $pK_a2 = 7.3 \pm 0.2$, and $pK_a3 = 9.6 \pm 0.6$. The isolated four spectral components of fluorescence emission (F^A, F^B, F^C, F^D) and of UV absorption ($F^{A'}$, $F^{B'}$, $F^{C'}$, $F^{D'}$) are shown in Figure 6.

In absorption, components $F^{A'}$ and $F^{B'}$ seem to be nearly identical. They are similar to the absorption spectrum of free Tyr and differ only by a multiplication factor close to unity. The $F^{D'}$ component resembles the spectrum of free tyrosinate. It does not correspond fully—we still observe some contribution of tyrosine. It is probably caused by the restriction of the upper pH limit of the measurement to 9.5 (due to the strong sample precipitation). The $F^{C'}$ component represents a state where a part of the tyrosines is converted into the tyrosinate form. We may consider two possible combinations: (i) 2 × Tyr and 1 × tyrosinate or (ii) 1 × Tyr and 2 × tyrosinate. The resulting spectra, given by such combination of $F^{B'}$ and $F^{D'}$ components, are drawn in Figure S2 in the Supporting Information. It is obvious that the variant i corresponds well, in contrast to the variant ii, to the spectral shape of the $F^{C'}$ component.

In fluorescence, the F^D component shows enormously low fluorescence; thus, it can be assigned to tyrosinate (consistently with absorption). When they are normalized, components F^C and F^B appear rather similar; however, F^C has notably stronger fluorescence above 330 nm (see Figure S3 in the Supporting Information). It points out that some of the tyrosines are transformed into the tyrosinate form. Similarly to absorption,

DOI: 10.1021/jp508897p
J. Phys. Chem. B 2015, 119, 1793–1801

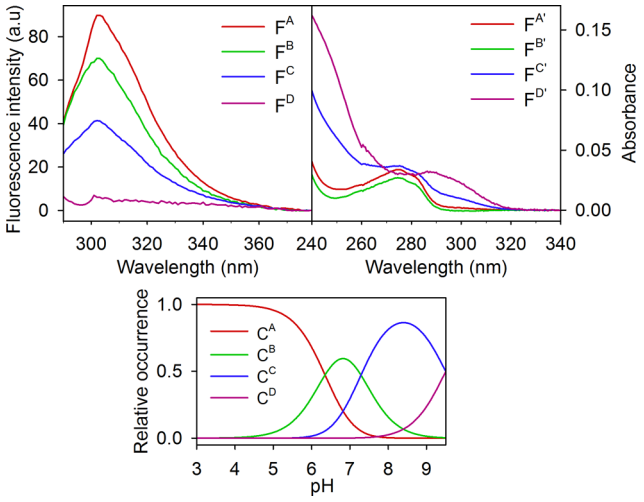

Figure 6. Absorption spectral components $F^{A'}$, $F^{B'}$, $F^{C'}$, and $F^{D'}$ (upper right) and fluorescence spectral components F^A, F^B, F^C, and F^D (upper left) extracted from the factor analysis of the pH titration of MADS^{SRF}. Relative occurrences of particular components at various pH's are shown in the lower graph.

the F^C component can be expressed as a linear combination of F^B and F^D components in the ratio corresponding to two tyrosines and one tyrosinate (see Figure S2 in the Supporting Information). Normalized components F^A and F^B differ in the region below 305 nm and around 315 nm, but they are nearly identical above 335 nm (see Figure 7). The difference (F^A − F^B) is characterized by an absence of a low frequency shoulder at 295 nm. A sharp increase is observed up to 304 nm (maximum), then a shoulder at 315 nm, and a subsequent decrease of the signal.

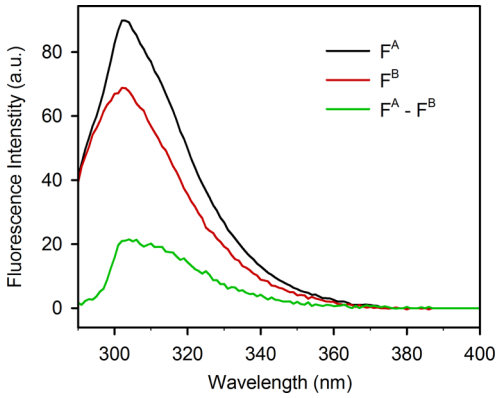

Figure 7. Fluorescence spectral components F^A and F^B from pH dependence and their difference F^A − F^B.

DISCUSSION

Structure Homology of MADS^{SRF}, Core-SRF, and Core-SRF/DNA Complex. In the X-ray structure of a complex of core-SRF (amino acids 124−245) with the DNA target, the MADS^{SRF} subpart possesses homologous secondary ordering in the C-terminal domain—the β-hairpin formed by sheets βI and βII and the N-terminal domain consists of a long helix αI and unordered extension (Figure 1). A corresponding secondary structure content of 37−39% β-sheet and 29−34% α-helix was also found for free core-SRF (amino acids 124−245) in aqueous solution.[14]

In contrast, our results (analysis of Raman amide I and III bands supported by CD measurements) show that in the case of the MADS^{SRF} domain alone (amino acids 142−197) only the structural elements folded in β-sheets (C-terminal part) are homologous with those of free core-SRF alone or of the specific core-SRF/DNA complex.[2,4,9] The MADS^{SRF} N-terminal part does not possess the stable α-helical structure found in both the free core-SRF and the complex, but it consists mainly of several short β-sheet segments. It is worth mentioning that this result is not in contradiction with the MADS^{SRF} primary sequence analysis using the Chou and Fasman[27] and GOR[28] algorithms, which predict that the C-terminal part (amino acids 181−197) folds into β-strands and adopts a β-hairpin-like topology, while the N-terminal part (amino acids 142−180) forms a strand of alternating short β-sheet and α-helical segments (Figure 1).

Very probably the αI SRF segment (amino acids 153−179) in isolated MADS^{SRF} does not possess a regular geometry and alternates between several conformations. On the other hand, the overall arrangement must be more compact than found for an isolated short oligopeptide from this segment (amino acids 168−175),[16] as the fluorescence results indicate shielding of both Tyr158 and Tyr173 (decreased quenching efficiency and lowered pK_a for Tyr158; see below).

The loss of the regular α-helical character between residues 153 and 179 is evidently caused by the shortening of the core-SRF sequence. It indicates that the MADS^{SRF} domain itself is flexible in its N-terminal part and requires at least intermolecular interactions with other parts of the core-SRF to stabilize the functional geometry.

Interpretation of Acid−Base Transition at pH 6.4. The first acido-basic transition with a pK_a1 = 6.4 ± 0.2 could be assigned to a deprotonation of His193. The pK_a of the free histidine side chain is 6.0;[35] this value can be higher when His is inside the peptide chain: The pK_a of His34 in wild-type apoflavodoxin is 6.36;[36] pK_a values of protein histidinyl residues in unfolded proteins were found in the interval 6.5−6.6.[37−39]

Changes in fluorescence and absorption spectral profiles, which enabled the pK_a1 determination, suggest that His193 has to be in some relation with one of the tyrosines serving as the inner probe. The most likely explanation is the existence of an internal H-bond between Tyr195 and His193. The tendency of Tyr to create a H-bond to the imidazole ring (which is a side chain of His) is well-known.[31,40] Existence of the hydrogen bond between Tyr195 and His193 is also apparent after addition of hydrogens to the published X-ray structure of the core-SRF/DNA target complex.[4] The corresponding bound pattern is (Tyr)O···H−N(His), where Tyr is an acceptor and His is a donor.[36] The distance of H···O is ca. 1.9 Å, which corresponds to the usual H-bond length (while the length of the chemical N−H bond is standard 1.01 Å). This is also in agreement with results derived from the shape and ratio of the tyrosine doublet I_{854}/I_{828} in the MADS^{SRF} Raman spectrum (see above).

Below the pH 6.4, the character of the His193−Tyr195 H-bond is somehow unusual in a sense that the histidine side chain is protonated and therefore positively charged. It is known that H-bonds between His and Tyr are stabilizing even in the case of a charged form of His (0.7 kcal/mol).[36] For the neutral form of His, the energy of the H-bond is higher (1.3 kcal/mol). Computations in a vacuum imply that the H-bond between Tyr and charged His is stronger due to more negative enthalpy;[41] however, this lowering of enthalpy is outweighed by a higher entropy (desolvation penalty). The positively charged

DOI: 10.1021/jp508897p
J. Phys. Chem. B 2015, 119, 1793−1801

His193 should affect the Tyr195 excited state and therefore also the band shape of its emission and excitation spectra. In Figure 3 (see also the "Tyr Fluorescence of MADS^{SRF}" section), the less complicated structure of the excitation spectrum at emission 293 nm indicates that Tyr195 involved in H-bonding to protonated His (pH 5.6) does not emit (or emits with low intensity) at this wavelength (see also the "Absorbance and Fluorescence pH Titration" section). Therefore, the 293 nm emission originates from the other two tyrosines that are H-bonded to water milieu. Complementarily, there is a fade-out of the fluorescence contribution ($F^A - F^B$) during the first acid−base transition which could be directly assigned to the change of the Tyr195 emission H-bonded to the either charged or uncharged His193. The ($F^A - F^B$) spectral shape (Figure 7) lacks the lower wavelength component at 293 nm which is consistent with the observations derived from excitation spectra. The respective absorption profiles before and after the His193 deprotonation, $F^{A'}$ and $F^{B'}$, remain unchanged, which indicates that the Tyr195 ground state is not affected.

Overall Outline of Acid−Base Transitions. On the basis of the conclusions mentioned above, the basic interpretation of the three acid−base transitions is possible. The first acid−base transition, given by pK_a1 = 6.4 ± 0.2, connected with minimal change in the absorption spectrum (i.e., only tyrosines are observed and no tyrosinate) and with a significant change in the fluorescence spectrum, can be assigned to deprotonation of His193. Between pK_a1 and pK_a2, all tyrosines remain in a neutral form, while two of them are H-bonded to the water milieu and one (Tyr195) to neutral His193. This is also in agreement with results derived from the shape and ratio of the tyrosine doublet in the Raman spectrum (see above). During the second acid−base transition with pK_a2 = 7.3 ± 0.2, one of the tyrosines is deprotonated. The last pK_a3 = 9.6 ± 0.6 corresponds to the transition of the remaining two tyrosines to tyrosinates. All observed acid−base transitions are schematically displayed in Figure 8.

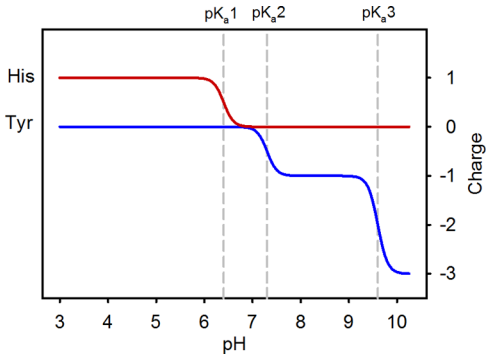

Figure 8. Most important changes of the MADS^{SRF} amino acid charges induced by alteration of the pH.

Interpretation of Acid−Base Transition at pH 7.3. The pK_a2 value obtained from pH titration revealed a considerable reduction in pK_a of one of the tyrosines (to 7.3) when compared to the pK_a of a free tyrosine (10.0). Such a low value can be caused either by the presence of charged groups in the Tyr vicinity or by a strong H-bond to the other residue. However, strong H-bonding was already excluded by Raman spectroscopy (see the "Raman Spectra of MADS^{SRF}" section). Therefore, the decrease in pK_a is probably caused by the presence of positively charged amino acids in proximity to tyrosine. This effect was described for the case of tyrosine in the vicinity of Lys or Arg residues in the literature.[42,43] In our previous work,[21] we discerned the pK_a of tyrosine residues within the short oligopeptide segment of MADS^{SRF} in the vicinity of Tyr158, $_{154}$KLRRYTTFS$_{162}$, and Tyr173, $_{168}$IMKKAYEL$_{175}$. The pK_a's of Tyr173 and Tyr158 were determined as 9.5 and 9.0, respectively. The decrease of the pK_a value of Tyr173 is caused by the proximity of two positively charged lysine residues (Lys170 and Lys171) and one negatively charged Glu174. The more significant decrease of the Tyr158 pK_a is caused by the imminent presence of two positively charged arginine residues (Arg156 and Arg157). The segment containing Tyr195 has not been separately studied, as it is predominantly hydrophobic (according to the Hopp−Woods hydrophobicity scale[3,44]).

The more significant decrease of the Tyr158 pK_a value[21] indicates that the pK_a2 constant determined from pH titration corresponds to this very residue. There is still the gap of 1.7 between pH 9.0 and 7.3. However, the secondary structures of shorter sequences are dominated by extended conformation[16] and substantially differ from the ordering in the β-sheet they possess as a part of the MADS box. This can lead to an additional decrease of pK_a values. Therefore, we conclude that deprotonation of Tyr158 is the most probable candidate for the acid−base transition at pH 7.3. More precise assignment of pK_a2 would require the use of site specific mutagenesis for preparation of MADS^{SRF} sequences with only one original tyrosine, while the remaining two would be substituted for, e.g., phenylalanines.

Interpretation of Quenching Experiment. On the basis of the results of pH titration, the emission spectrum of MADS^{SRF} measured at pH 6.5 has several contributions emerging from (a) Tyr195 H-bonded to charged His193, (b) Tyr195 H-bonded to neutral His193, and (c) the other two tyrosines in the neutral state H-bonded to water milieu. Due to pH close to pK_a1, the amount of (a) and (b) is comparable. Moreover, ca. 15% of one of the tyrosines is in the form of tyrosinate due to the proximity of pK_a2. However, the factor analysis of quenching experiments shows only two different components F_I and F_{II}.

Nevertheless, it seems that we can show the coherence of results obtained from the quenching and titration experiments, which supports the reliability of the experimental data and their interpretation. As shown in Figure S4 in the Supporting Information, the F_I component from quenching is similar to the difference ($F^A - F^B$) from pH measurements (that corresponds to the transition between the charged and neutral forms of His193). The F_{II} component from quenching is then similar to the F^B component from pH experiment (His193 and all Tyr in the neutral state). Resemblance to the component F^C can be excluded, as F_{II} does not manifest any increase of fluorescence in the region 315−360 nm.

Therefore, the more efficiently quenched F_I component can be assigned to Tyr195 interacting by a H-bond with charged His193, while the less efficiently quenched F_{II} component corresponds to all other tyrosines (i.e., Tyr195 H-bonded to the neutral His193 and the other two tyrosines Tyr158 and Tyr173). The fact that these tyrosines form only one SVD component suggests that they all have about the same emission spectrum.

As the overall fluorescence spectrum of MADS^{SRF} is a sum of components F_I and F_{II}, the shoulder on the shorter wavelength of its three humped emission spectrum (Figure 3) does not

DOI: 10.1021/jp508897p
J. Phys. Chem. B 2015, 119, 1793−1801

contain (or contains only negligibly) any contribution from Tyr195 H-bonded to charged His193, which is in good agreement with the observation based on excitation spectra.

Role of His193. Our results have revealed an acido-basic transition in MADS^{SRF} characterized by pK_a ≈ 6.4, which corresponds to deprotonation of His193 in the C-terminal part, connected by a hydrogen bond with Tyr195. The MADS^{SRF} C-terminal domain in a β-hairpin fold, i.e., two β-strands joined by a β-loop (containing His193), forms a hydrophobic core centered on the conserved hexameric sequence $_{183}$VLLLVA$_{188}$.[13] In the complexes between core-SRF and target oligonucleotide, some residues of the β-hairpin (including His193) serve as direct contact points with phosphate groups at the edge of the target SRE segment.[4,8,9] The DNA target is continuously switching between bend and linear conformers[14,15] exposing the β-loop to the variations of structural constraints and charges. The C-terminal domain is also involved in core-SRF dimerization which is imperative for the correct DNA target binding.[4] Specifically, the assembly of the protein dimer is strongly connected to the repartition of the electrostatic charges on the protein during the core-SRF/DNA target complex formation.[14] The high level of hydrophobic residues of MADS^{SRF}, i.e., a C-terminal hydrophobic core and an amphipathic N-terminal domain, favors intermolecular interactions. They can be presumably altered by His193 charge variation even in the absence of MADS^{SRF} structural changes. Therefore, it could be supposed that the charge variation of the β-loop caused by His193 plays a significant role in the behavior of the hydrophobic C-terminal domain. We should recall that the C-terminal part of MADS (SRF 142−197) has a similar structure to core-SRF, whereas the N-terminal part does not have its structure. This pinpoints the specific role of the charge in the hydrophobic C-terminal part, at least in the dimerization process.

Evolutionarily, MADS sequences originated from a region of the topoisomerase II A subunit (TopoIIA-A).[2] MADS proteins gained sequence specificity in DNA binding after they branched off from TopoIIA-A. DNA specificity acquisition required an integrated process involving join coevolution between the N-terminal DNA binding domain and the C-terminal dimerization domain. The presence of His193 in the β-loop results from that process, and it can be found in all Metazoans (and predominantly in Unikonts).[2,45]

CONCLUSIONS

We may conclude that His193 acts as a sensor and mediator of the electrostatic interactions developed by the N-terminal binding domain to have repercussion on the C-terminal dimerization domain, and is indispensable for the SRF specificity. Thus, in MADS sequences, the β-loop with its charged residues can play a significant role in the DNA specific recognition.

ASSOCIATED CONTENT

Supporting Information

Figures of the factor analysis of both fluorescence and absorption spectra of MADS^{SRF} pH titration and comparison of the various absorption and fluorescence spectral components. This material is available free of charge via the Internet at http://pubs.acs.org.

AUTHOR INFORMATION

Corresponding Author

*Phone: +420-221 911 345. Fax: +420-224 922 797. E-mail: stepjos@karlov.mff.cuni.cz.

Author Contributions

Y.-M.C. provided the samples; B.A. and C.Z. proposed a strategy of experiments; B.P., V.K., J.S., and C.Z. measured and processed spectra; B.P., J.S., V.P., V.K., P.-Y.T., and C.Z. analyzed and interpreted data; B.P. and V.P. created the figures; B.P., V.P., V.K., J.S., and C.Z. wrote the manuscript; all authors discussed the manuscript together.

Notes

The authors declare no competing financial interest.

ACKNOWLEDGMENTS

This work was supported by the Czech Science Foundation (202/09/0193) and the Grant Agency of Charles University (No. 402111). B.P. gratefully acknowledges the French Government support for her stay in Laboratoire Jean Perrin (Université Pierre et Marie Curie, France). The authors thank Dr. Kateřina Hofbauerová and Vlastimil Zíma (Institute of Physics, Charles University in Prague) for electrophoretic checking of the peptide samples and molecular dynamic simulations, respectively. We also highly appreciate the measurements of circular dichroism spectra by Dr. Lucie Bednárová (Institute of Organic Chemistry and Biochemistry, Academy of Sciences of the Czech Republic).

ABBREVIATIONS

CD, electronic circular dichroism; FA, factor analysis; MADS^{SRF}, SRF MADS box; MPLC, medium pressure liquid chromatography; RP-HPLC, reverse-phase high pressure liquid chromatography; SRF, serum response factor; SVD, singular value decomposition

REFERENCES

(1) Schwarz-Sommer, Z.; Huijser, P.; Nacken, W.; Saedler, H.; Sommer, H. Genetic control of flower development by homeotic genes in *Antirrhinum majus*. *Science* **1990**, *250*, 931−936.

(2) Gramzow, L.; Ritz, M. S.; Theissen, G. On the origin of MADS-domain transcription factors. *Trends Genet.* **2010**, *26*, 149−153.

(3) Shore, P.; Sharrocks, A. D. The MADS-box family of transcription factors. *Eur. J. Biochem.* **1995**, *229*, 1−13.

(4) Pellegrini, L.; Tan, S.; Richmond, T. J. Structure of serum response factor core bound to DNA. *Nature* **1995**, *376*, 490−498.

(5) Tan, S.; Richmond, T. J. Crystal structure of the yeast MATα2/MCM1/DNA ternary complex. *Nature* **1998**, *391*, 660−666.

(6) Huang, K.; Louis, J. M.; Donaldson, L.; Lim, F. L.; Sharrocks, A. D.; Clore, G. M. Solution structure of the MEF2A-DNA complex: structural basis for the modulation of DNA bending and specificity by MADS-box transcription factors. *EMBO J.* **2000**, *19*, 2615−2628.

(7) Santelli, E.; Richmond, T. J. Crystal structure of MEF2A core bound to DNA at 1.5 Å resolution. *J. Mol. Biol.* **2000**, *297*, 437−449.

(8) Hassler, M.; Richmond, T. J. The B-box dominates SAP-1 interactions in the structure of the ternary complex. *EMBO J.* **2001**, *20*, 3018−3028.

(9) Mo, Y.; Ho, W.; Johnston, K.; Marmorstein, R. Crystal structure of a ternary SAP-1/SRF/c-fos SRE DNA complex. *J. Mol. Biol.* **2001**, *314*, 495−506.

(10) Nurrish, S. J.; Treisman, R. DNA binding specificity determinants in MADS-box transcription factors. *Mol. Cell. Biol.* **1995**, *15*, 4076−4085.

(11) Norman, C.; Runswick, M.; Pollock, R.; Treisman, R. Isolation and properties of cDNA clones encoding SRF, a transcription factor

DOI: 10.1021/jp508897p
J. Phys. Chem. B 2015, 119, 1793−1801

that binds to the *c*-fos serum response element. *Cell* **1988**, *55*, 989−100.
(12) Hipskind, R. A.; Rao, V. N.; Mueller, C. G. F.; Reddy, E. S. P.; Nordheim, A. Ets-related protein Elk-1 is homologous to the *c*-fos regulatory factor p62TCF. *Nature* **1991**, *354*, 531−534.
(13) Sharrocks, A. D.; Gille, H.; Shaw, P. E. Identification of amino acids essential for DNA binding and dimerization in p67SRF: implication for a novel DNA-binding motif. *Mol. Cell. Biol.* **1993**, *13*, 123−132.
(14) Štěpánek, J.; Kopecký, V., Jr.; Mezzetti, A.; Turpin, P.-Y.; Paulin, D.; Alpert, B.; Zentz, C. Structural and dynamic changes of the serum response element and the core domain of serum response factor induced by their association. *Biochem. Biophys. Res. Commun.* **2010**, *391*, 203−208.
(15) Štěpánek, J.; Kopecký, V., Jr.; Turpin, P.-Y.; Li, Z.; Alpert, B.; Zentz, C. DNA electric charges oscillations govern protein-DNA recognition. *PLoS One* **2015**, submitted for publication.
(16) Profantová, B.; Profant, V.; Zíma, V.; Kopecký, V., Jr.; Bednárová, L.; Zentz, C.; Baumruk, V.; Turpin, P.-Y.; Štěpánek, J. Protonation effect of tyrosine in a segment of the SRF transcription factor: a combined optical spectroscopy, molecular dynamics, and density functional theory calculation study. *J. Phys. Chem. B* **2013**, *117*, 16086−16095.
(17) Chan, W. C.; White, P. D. *Fmoc Solid Phase Peptide Synthesis: A Practical Approach*; Oxford University Press: London, 2000.
(18) Lakowicz, J. R. *Principles of Fluorescence Spectroscopy*, 3rd ed.; Springer: Singapore, 2006.
(19) Malinowski, E. R. *Factor Analysis in Chemistry*, 3rd ed.; Wiley: New York, 2002.
(20) Stern, O.; Volmer, M. Über die abkingzeit der fluoreszenz. *Phys. Z.* **1919**, *20*, 183−188.
(21) Řezáčová, B.; Coïc, Y.-M.; Zentz, C.; Turpin, P.-Y.; Štěpánek, J. Spectroscopic determination of pK_a constants of MADS box segments. *Spectrosc. Int. J.* **2012**, *27*, 455−461.
(22) Tensmeyer, L. G.; Kauffman, E. W., Jr. Protein structure as revealed by nonresonance Raman spectroscopy. In *Spectroscopic Methods for Determining Protein Structure in Solution*; Havel, H. A., Ed.; VCH: New York, 1996; pp 69−95.
(23) Overman, S. A.; Thomas, G. J., Jr. Raman markers of nonaromatic side chains in an α-helix assembly: Ala, Asp, Glu, Ile, Lys, Ser, and Val residues of phage *fd* subunits. *Biochemistry* **1999**, *38*, 4018−4027.
(24) Tuma, R. Raman spectroscopy of proteins: from peptides to large assemblies. *J. Raman Spectrosc.* **2005**, *36*, 307−319.
(25) Siamwiza, M. N.; Lord, R. C.; Chen, M. C. Interpretation of the doublet at 850 and 830 cm^{-1} in the Raman spectra of tyrosyl residues in proteins and certain model compounds. *Biochemistry* **1975**, *14*, 4870−4876.
(26) Williams, R. W. The secondary structure analysis using Raman amide I and amide III spectra. *Methods Enzymol.* **1986**, *130*, 311−331.
(27) Chou, P.-Y.; Fasman, G. D. Prediction of protein conformation. *Biochemistry* **1974**, *13*, 222−245.
(28) Garnier, J.; Gibrat, J.-F.; Robson, B. GOR secondary structure prediction method version IV. *Methods Enzymol* **1996**, *266*, 540−553.
(29) Atkins, W. M.; Dietze, E. C.; Ibarra, C. Pressure-dependent ionization of Tyr 9 glutathione S-transferase A1−1: contribution of the C-terminal helix to a "soft" active site. *Protein Sci.* **1997**, *6*, 873−881.
(30) Dietze, E. C.; Wang, R. W.; Lu, A. Y. H.; Atkins, W. M. Ligand effects on the fluorescence properties of tyrosine-9 in alpha 1−1 glutathione S-transferase. *Biochemistry* **1996**, *35*, 6745−6753.
(31) Ross, J. B. A.; Laws, W. R.; Rousslang, K. W.; Wyssbrod, H. R. In *Topics in Fluorescence Spectroscopy*; Lakowicz, J., Ed.; Plenum Press: New York, 1992; Vol. 3, pp 1−54.
(32) Patterson, L. K.; Rzad, S. J. Quenching of aromatic hydrocarbon fluorescence by cesium-chloride. *Chem. Phys. Lett.* **1975**, *31*, 254−256.
(33) Texier, I.; Berberan-Santos, M. N.; Fedorov, A.; Brettreich, M.; Schönberger, H.; Hirsch, A.; Leach, S.; Besasson, R. V. Photophysics and photochemistry of a water-soluble C-60 dendrimer: Fluorescence quenching by halides and photoinduced oxidation of I^-. *J. Phys. Chem. A* **2001**, *105*, 10275−10285.
(34) Homer, R. B.; Allsopp, S. R. An investigation of the electronic and steric environment of tyrosyl residues in ribonuclease a and Erwinia Caroto-voral-asparaginase through fluorescence quenching by caesium, iodide and phosphate. *Biochim. Biophys. Acta* **1976**, *434*, 297−310.
(35) Lehninger, A. L.; Nelson, D. L.; Cox, M. M. *Lehninger Principles of Biochemistry*, 4th ed.; W. H. Freeman: New York, 2005.
(36) Fernandez-Recio, J.; Romero, A.; Sancho, J. Energetics of a hydrogen bond (charged and neutral) and of a cation-π interaction in apoflavodoxin. *J. Mol. Biol.* **1999**, *290*, 319−330.
(37) Matthews, C. R.; Westmoreland, D. G. Nuclear magnetic resonance studies of residual structure in thermally unfolded ribonuclease A. *Biochemistry* **1975**, *14*, 4532−4538.
(38) Anderson, D. E.; Becktel, W. J.; Dahlquist, F. W. pH-induced denaturation of proteins: a single salt bridge contributes 3−5 kcal/mol to the free energy of folding of T4 lysozyme. *Biochemistry* **1990**, *29*, 2403−2408.
(39) Sancho, J.; Serrano, L.; Fersht, A. R. Histidine residues at the N- and C-termini of α-helices: perturbed pK_as and protein stability. *Biochemistry* **1992**, *31*, 2253−2258.
(40) Willis, K. J.; Szabo, A. G. The fluorescence dacay kinetics of tyrosinate and tyrosine hydrogen bonded complexes. *J. Phys. Chem.* **1991**, *95*, 1585−1589.
(41) Weiner, S. J.; Kollman, P. A.; Case, D. A.; Singh, U. C.; Ghio, C.; Alagona, G.; Profeta, S.; Weiner, P. A new force-field for molecular mechanical simulation of nucleic-acids and proteins. *J. Am. Chem. Soc.* **1984**, *106*, 765−784.
(42) Sella, M.; Katchalski, E. Spectrophotometric titration α-amino acid copolymers containing tyrosine. *J. Am. Chem. Soc.* **1956**, *78*, 3986−3989.
(43) Vinograd, S. N.; Linnel, R. H. The hydrogen bond in biological materials. *Hydrogen Bonding*; Van Nostrand Reinhold: New York, 1971; pp 223−254.
(44) Hopp, T. P.; Woods, K. R. Prediction of protein antigenic determinants from amino acid sequences. *Proc. Natl. Acad. Sci. U.S.A.* **1981**, *78*, 3824−3828.
(45) Cavalier-Smith, T. The phagotrophic origin of eukaryotes and phylogenetic classification of Protozoa. *Int. J. Syst. Evol. Microbiol.* **2002**, *52*, 297−354.

DOI: 10.1021/jp508897p
J. Phys. Chem. B 2015, 119, 1793−1801